Luigi Grazioli, MD
Giovanni Morana, MD
Miles A. Kirchin, PhD
Günther Schneider, MD

Published online before print
10.1148/radiol.2361040338
Radiology 2005; 236:166–177

Abbreviations:
BOPTA = benzyloxypropionictetraacetate
FNH = focal nodular hyperplasia
GRE = gradient echo
HA = hepatic adenoma
LA = liver adenomatosis
RARE = rapid acquisition with relaxation enhancement
VIBE = volumetric interpolated breath-hold examination

[1] From the Department of Radiology, University of Brescia, Spedali Civili di Brescia, Piazzale Spedali Civili 1, 25023 Brescia, Italy (L.G.); Department of Diagnostic Radiology, Ospedale Cà Foncello, Treviso, Verona, Italy (G.M.); Worldwide Medical Affairs, Bracco Imaging, Milan, Italy (M.A.K.); and Department of Diagnostic Radiology, University Hospital, Homburg/Saar, Germany (G.S.). Received February 20, 2004; revision requested April 29; revision received July 15; accepted September 2. **Address correspondence to** L.G. (e-mail: *lgrazioli@yahoo.com*).

See Materials and Methods for pertinent disclosures.

Author contributions:
Guarantors of integrity of entire study, L.G., G.M., G.S.; study concepts and design, all authors; literature research, M.A.K.; clinical studies, L.G., G.M., G.S.; data acquisition and analysis/interpretation, all authors; manuscript preparation, editing, and final version approval, M.A.K.; manuscript definition of intellectual content and revision/review, all authors

Accurate Differentiation of Focal Nodular Hyperplasia from Hepatic Adenoma at Gadobenate Dimeglumine–enhanced MR Imaging: Prospective Study[1]

PURPOSE: To prospectively determine the accuracy of differentiating benign focal nodular hyperplasia (FNH) from hepatic adenoma (HA) and liver adenomatosis (LA) by using gadobenate dimeglumine–enhanced magnetic resonance (MR) imaging.

MATERIALS AND METHODS: The ethics committee at each center approved the study, and all patients provided informed consent. Seventy-three patients with confirmed FNH and 35 patients with confirmed HA (n = 27) or LA (n = 8) underwent MR imaging before (T2-weighted half-Fourier rapid acquisition with relaxation enhancement or T2-weighted fast spin-echo and T1-weighted gradient-echo [GRE] sequences) and at 25–30 seconds (arterial phase), 70–90 seconds (portal venous phase), 3–5 minutes (equilibrium phase), and 1–3 hours (delayed phase) after (T1-weighted GRE sequences only, with or without fat suppression) bolus administration of 0.1 mmol per kilogram of body weight gadobenate dimeglumine. The enhancement of 235 lesions (128 FNH, 32 HA, and 75 LA lesions) relative to the normal liver parenchyma was assessed. Sensitivity, specificity, positive predictive value (PPV), negative predictive value (NPV), and overall accuracy for the differentiation of FNH from HA and LA were determined.

RESULTS: Hyper- and isointensity on T2-weighted and iso- and hypointensity on T1-weighted GRE images were noted for 177 (88.9%) of 199 lesions visible on unenhanced images. On dynamic phase images after contrast material administration, 231 (98.3%) of 235 lesions showed rapid strong enhancement during the arterial phase and appeared hyper- to isointense during portal venous and equilibrium phases. Accurate differentiation of FNH from HA and LA was not possible on the basis of precontrast or dynamic phase images alone. At 1–3 hours after contrast material enhancement, 124 (96.9%) of 128 FNHs appeared hyper- or isointense, while 107 (100%) HA and LA lesions appeared hypointense. The sensitivity, specificity, PPV, NPV, and overall accuracy for the differentiation of FNH from HA and LA were 96.9%, 100%, 100%, 96.4%, and 98.3%, respectively.

CONCLUSION: Accurate differentiation of FNH from HA and LA is achievable on delayed T1-weighted GRE images after administration of gadobenate dimeglumine.

Focal nodular hyperplasia (FNH) is a benign tumorlike hepatic lesion that is believed to be the result of a hyperplastic response to abnormal vasculature (1). Histologically, it is characterized by the presence of normal hepatocytes with a malformed biliary system that leads to a slowing of biliary excretion (2). Since FNH is not associated with any malignant potential (1,3,4) and has only a minimal tendency for rupture and hemorrhage (4,5), confirmed FNH is almost always managed conservatively (4,6–10). Hepatic adenoma (HA) is also considered a benign hepatocellular lesion. However, unlike FNH, HA is frequently

a candidate for surgical resection because of a marked tendency for rupture and hemorrhage, with subsequent bleeding into the normal liver or abdominal cavity, and because of a potential for malignant transformation (3,4,7–17).

Frequently, the diagnosis of FNH or HA can be aided by the presence of characteristic lesion features such as a central scar in the case of FNH (18–20) or a heterogeneous appearance due to intralesional hemorrhage in the case of HA (11,18,19,21). However, these features are not present in every nodule and have often been reported in fewer than 50% of FNH and HA lesions (11,16,20,22). Although previous studies in which a variety of diagnostic procedures have been used have demonstrated accuracy of up to approximately 90% for the differential diagnosis of FNH and HA (3,8,9,17,23), the accurate differentiation of these lesions remains problematic in the absence of histologic results from lesion biopsy (6,8,9,24). However, lesion biopsy may represent an increased risk in patients with HA because of the increased possibility of hemorrhage (3,10). The difficulty of differential diagnosis of FNH and HA is further compounded by the fact that both types of lesion typically occur in women of child-bearing potential, who may be asymptomatic, and with a history of oral contraceptive use (3,4, 6,19). Because the formal diagnosis of these lesions usually results in different approaches to patient management and treatment, their accurate differentiation with noninvasive diagnostic imaging, leading to a redundant need for lesion biopsy, is highly desirable.

Currently, contrast material–enhanced magnetic resonance (MR) imaging is considered a highly accurate diagnostic procedure for the detection and characterization of focal liver lesions (25) and is often used as a problem-solving modality when equivocal findings are obtained with other imaging techniques (9,10). Unfortunately, the enhancement behavior of FNH and HA, particularly in small atypical lesions that do not have a central scar (in the case of FNH) or are nonhemorrhagic (in the case of HA), may be similar. Typically, both types of lesion demonstrate strong enhancement during the arterial phase after bolus administration of a conventional extracellular gadolinium-based contrast agent followed by moderate hyperintensity or isointensity during the subsequent portal venous and equilibrium phases. A similar pattern of enhancement has been noted on computed tomographic (CT) scans after administration of iodinated contrast agents (26).

Gadobenate dimeglumine (MultiHance; Bracco Imaging, Milan, Italy) is a gadolinium-based contrast agent that is approved in Europe and other countries of the world for MR imaging of the central nervous system and the liver and in the United States for MR imaging of the central nervous system. Gadobenate dimeglumine differs from conventional gadolinium-based agents in that it possesses a two-fold greater T1 relaxivity in human plasma (9.7 $L \cdot mmol^{-1} \cdot sec^{-1}$ at 0.47 T) because of weak and transient interaction of the gadolinium (Gd)-benzyloxypropionictetraacetate (BOPTA) contrast-effective moiety with serum albumin (27–29), and because it undergoes elimination from the body through both the renal (95%–97% of injected dose) and hepatobiliary (3%–5% of injected dose) pathways (29,30). The hepatobiliary elimination appears to occur as a result of functioning hepatocytes taking up the Gd-BOPTA chelate of gadobenate dimeglumine and eliminating it via an anionic transporter across the sinusoidal membrane into the bile (31,32). It can be seen on T1-weighted images as a marked and long-lasting enhancement of the normal liver parenchyma (33) against which metastases and primary hepatic malignant lesions typically appear hypointense because of the absence of functioning hepatocytes, while FNH and other benign lesions appear iso- or slightly hyperintense (34–36). However, the situation may be different for HAs since these lesions lack bile ducts (2,18) and thus may have altered hepatobiliary metabolism, which results in the absence of Gd-BOPTA uptake and transport compared with that occurring in other benign hepatocellular lesions. Similarly, liver adenomatosis (LA) lesions are histologically and radiologically identical to HAs (18,37,38). Thus, our study was performed to prospectively determine the accuracy of differentiating benign FNH from HA and LA by using gadobenate dimeglumine–enhanced MR imaging.

MATERIALS AND METHODS

Study Population

A total of 73 patients (64 women, nine men; mean age, 38.1 years ± 10.5 [± standard deviation]; range, 21–61 years) with one (n = 51) or multiple (n = 22) FNHs; 27 patients (22 women, five men; mean age, 39.4 years ± 13.3; range 13–64 years) with one (n = 23), two (n = 3), or three (n = 1) HAs; and eight patients (seven women, one man; mean age, 39.8 years ± 6.8; range, 28–50 years) with LA lesions were prospectively studied at three centers in Europe. There were no significant differences between the group of patients with FNH and the group of patients with HA and LA lesions either in terms of the age of the evaluated subjects (P = .604, Student t test) or the distribution of men and women (P = .518, Fisher exact test). However, the proportion of women to men in each group was significantly different ($P < .001$ for the FNH group and P = .001 for the HA and LA group, χ^2 test), which reflects a greater prevalence of these lesions among the female population (3,6,9,24).

Patients were included for evaluation in a consecutive manner at each center on the basis of the final diagnosis of the investigating radiologist (L.G., G.M., or G.S., each with more than 12 years of experience in liver MR imaging and 8 years of experience in liver MR imaging specifically with gadobenate dimeglumine). All patients were included as part of routine clinical practice. In most cases, patients were referred for MR imaging either to confirm a previous diagnosis or because they were returning for follow-up examinations of a previously diagnosed lesion. To prevent the possibility of selection bias, all patients with a lesion diagnosed as FNH or HA and LA who were examined during the specified period of the study were included in the evaluation. Patients with FNH were examined between January and September 2003, including 10 patients returning for follow-up MR examinations for previously diagnosed FNH. Patients with HA and LA were examined over a longer period of time (between March 1999 and September 2003), which reflects the rarer incidence of these lesions. The ethics committee at each center approved the study. All patients provided informed consent. All data and information derived from and pertaining to the study were under the exclusive control of the investigating radiologists. Author M.A.K., an employee of Bracco, did not have control over any data or information and played no part in patient enrolment or examination.

Of the 73 patients with FNH, 12 (16.4%) had pain in the upper abdomen. The remaining 61 patients were asymptomatic; the presence of FNH in these patients was an incidental finding at abdominal imaging performed for other reasons. Among the 35 patients with HA or LA, 21 patients had chronic upper

quadrant pain and 14 were asymptomatic. Twenty-three of the 64 female patients with FNH, 13 of the 22 female patients with HA, and five of the seven female patients with LA had a history of taking oral contraceptives. None of the male patients in the study were taking steroids. Among the patients with FNH, five patients had a history of breast cancer, two patients had a history of melanoma, one patient had a history of pulmonary carcinoid, one patient had a history of endometrial carcinoma, and one patient had a history of retroperitoneal Schwannoma infiltrating the kidneys. Among the patients with HA or LA, one patient had a history of thyroid cancer, one patient had hepatitis C, one patient had a history of ulcerative colitis, one patient had hypertension, and one patient had perinatal thrombosis of the portal vein.

A total of 128 FNH (mean size, 33.3 mm ± 22.4; including three FNH lesions in patients with HA or LA), 32 HA (mean size, 59.2 mm ± 45.1), and at least 106 LA lesions were detected in the 108 patients included in the study. For the patients with LA lesions, only lesions measuring 10 mm or greater with available histologic results after liver transplantation ($n = 1$) or percutaneous biopsy ($n = 7$) in at least three lesions per patient were considered. The number of LA lesions evaluated in the study was 75 (mean size, 23.0 mm ± 16.3), which resulted in a total of 235 evaluable lesions.

Confirmation of lesions was performed after surgical resection (two FNHs in two patients, 19 HAs in 17 patients), percutaneous biopsy (39 FNHs in 29 patients plus one FNH in one patient with LA, 13 HAs in 10 patients, and 27 lesions in seven patients with LA), intraoperative ultrasonography (two FNHs in one patient undergoing resection for solitary HA), or orthotopic liver transplantation (six lesions in one patient with LA). The remaining patients underwent some other prior diagnostic imaging procedure (technetium 99m diethyl-iminodiacetic acid nuclear medicine scan, 11 FNHs in seven patients; or helical CT, 73 FNHs in 35 patients), with the final diagnosis reached on the basis of all available imaging findings.

MR Imaging Protocol

The same MR imaging protocol was used in each institution. All patients were imaged with a superconducting imager (Magnetom Symphony or Magnetom Vision; Siemens Medical Systems, Erlangen, Germany) operating at 1.5 T by using a body-array coil. MR imaging was performed by using T2-weighted turbo spin-echo sequences with or without fat saturation (repetition time msec/echo time msec, 4000/90–108; flip angle, 150°; echo train length, 29) or T2-weighted half-Fourier rapid acquisition with relaxation enhancement (RARE) (HASTE; Siemens Medical Systems) sequence (∞/74, 180° flip angle) and T1-weighted gradient-echo (GRE) in-phase (140–160/4.7, 70° flip angle) and out-of-phase (140–160/2.6, 70° flip angle) sequences or T1-weighted volumetric interpolated breath-hold examination (VIBE) (6.2/2.5, 15° flip angle). Images were acquired prior to the administration of contrast agent (T2-weighted fast spin-echo and T1-weighted GRE or VIBE images); during the dynamic phase of contrast enhancement (T1-weighted GRE or VIBE images only) at 25–30 seconds (arterial phase), 70–90 seconds (portal venous phase), and 3–5 minutes (equilibrium phase) following intravenous bolus (2–2.5 mL/sec) administration of gadobenate dimeglumine at a dose of 0.1 mmol per kilogram of body weight; and during a later delayed hepatobiliary phase (T1-weighted GRE images only) at one or more time points between 1 and 3 hours after injection. Postcontrast delayed phase images were acquired with and without fat suppression. The section thickness was 6 mm for unenhanced images and images acquired during the delayed phase and between 6 and 10 mm, depending on the hepatic volume, for images acquired during the postcontrast dynamic phase. T2-weighted half-Fourier RARE images of the entire liver were acquired either in a single slab with a total breath-hold acquisition time of 19–21 seconds or in two slabs of 11 sections with an acquisition time of 14 seconds each. T2-weighted fast spin-echo and T1-weighted GRE images of the entire liver were acquired in single breath-hold acquisitions of 19–23 seconds. The T1-weighted VIBE images were acquired with a single breath-hold acquisition of 18 seconds. A matrix size of 160 × 256 was used with a rectangular field of view of 350–420 mm.

Image Analysis

Images were evaluated in consensus by three investigating radiologists (L.G., G.M., G.S.) in terms of the intensity and homogeneity of the lesion signal intensity on in-phase MR images acquired before contrast agent administration and during the dynamic and delayed phases of the MR study. Images were also evaluated for the presence of a central scar or atypical lesion features. The signal intensity was considered homogeneous when equal signal intensity was observed in all parts of the lesion with the exception of the central scar, if present. In each case, assessment of images from each patient was performed in a similar manner to that which occurs in routine practice, with all image sets available for simultaneous evaluation. The three readers in consensus were required merely to designate each detected lesion as hypointense, isointense, or hyperintense to the surrounding normal liver parenchyma and to decide whether the lesion was homogeneous and possessed a central scar or not. Thus, while in all cases two of the three readers were blinded to all the details of a given case and to the final diagnosis of the lesion, there was no diagnostic element to the evaluation procedure and no requirement for readers to state whether a lesion was an FNH, HA, or LA. Matching of the lesion enhancement patterns with the final diagnosis of the lesions was performed subsequently, after image evaluation was complete.

On the basis of features observed on precontrast and dynamic phase images and of prior reports of the appearance and enhancement characteristics of FNH (17,19,26,36), lesions diagnosed as FNH were defined as either typical or atypical. Lesions were considered typical when they appeared homogeneously isointense or slightly hyperintense with respect to the normal surrounding liver parenchyma on T2-weighted fast spin-echo images and isointense or slightly hypointense on T1-weighted GRE images before administration of gadobenate dimeglumine. Typical behavior during the dynamic phase of contrast enhancement was noted when the lesion demonstrated marked and homogeneous signal intensity enhancement during the arterial phase, rapid and homogeneous signal intensity washout during the portal venous phase, and signal isointensity during the equilibrium phase. A typical scar was revealed as a hyperintense central stellate area on T2-weighted fast spin-echo images and as a hypointense area on T1-weighted GRE images. During the dynamic phase of contrast enhancement, a typical scar appeared hypointense during the arterial and portal venous phases and slightly hyperintense during the equilibrium phase. The presence of a scar was considered necessary for the definition of a typical lesion only for lesions greater than 3 cm in size.

Atypical features of FNH consisted of the following: lesion heterogeneity, hypointensity in the portal venous or equilibrium phases, absence of a central scar in lesions greater than 3 cm, scar hypointensity on T2-weighted fast spin-echo images, and scar hypointensity in the equilibrium phase following contrast agent injection. Other atypical features were the presence of a pseudocapsule, which was observed as a complete hyperintense perilesional ring during the equilibrium phase, the presence of hemorrhage, and the presence of necrosis.

As in the case of FNH, typical features of HA and LA lesions were iso- or slight hyperintensity with respect to the normal surrounding liver parenchyma on precontrast T2-weighted fast spin-echo images and iso- or slight hypointensity on T1-weighted GRE images, possibly with areas of increased signal intensity due to the presence of fat and/or subacute hemorrhage and areas of reduced signal intensity due to necrosis or old hemorrhage (17,19,21,37,39). On dynamic phase images after the injection of gadobenate dimeglumine, typical HA and LA lesions demonstrated marked signal intensity enhancement during the arterial phase, followed by persisting hyperintensity during the portal venous phase and slight hyperintensity or isointensity to the normal liver parenchyma during the equilibrium phase. Other features observed during dynamic imaging that were considered typical, of larger HA in particular, were focal heterogeneous nonenhancing hypointense areas corresponding to areas of necrosis, calcification, or fibrosis.

On delayed images after gadobenate dimeglumine administration, typical FNHs have been reported to have an isointense or hyperintense appearance relative to the surrounding normal liver parenchyma, while preliminary experience has suggested that HA and LA lesions have a marked hypointense appearance (36). A hypointense central scar is also typical of FNH on postcontrast delayed MR images (36).

Statistical Analysis

The sensitivity, specificity, positive predictive value, negative predictive value, and overall accuracy for the differentiation of FNH from HA and LA lesions were determined on the basis of postcontrast lesion enhancement patterns on delayed MR images. A true-positive lesion was a lesion with a final diagnosis of FNH and was isointense or hyperintense to the surrounding liver parenchyma, a true-negative lesion was a lesion with a final diagnosis of HA or LA and was hypointense to the surrounding liver parenchyma, a false-positive lesion was a lesion with a final diagnosis of HA or LA and was isointense or hyperintense to the surrounding liver parenchyma, and a false-negative lesion was a lesion with a final diagnosis of FNH and was hypointense to the surrounding liver parenchyma.

The results of delayed phase imaging were analyzed with the χ^2 test to determine the significance of the differences in the signal intensity between FNH and HA and LA lesions. A possible correlation between multiple lesions in individual subjects was taken into consideration by performing an additional χ^2 test of just a single lesion in these patients and by using generalized estimating equation methods with a level of significance of $P < .05$.

The power of the study for an equal proportion of hypointense lesions was determined with the χ^2 test. Assuming that 90% of FNH lesions and 10% of HA and LA lesions would be classified as either hyperintense or isointense, we calculated that the study power would exceed 99% with 100 lesions in each group by using a two-sided test with an α level of .05. All analyses were performed with SAS software (version 8.2; SAS Institute, Cary, NC).

RESULTS

The enhancement behavior of the lesions on precontrast and postcontrast dynamic and delayed phase images is shown in the Table.

Precontrast Unenhanced Imaging

On precontrast T2-weighted fast spin-echo or T2-weighted half-Fourier RARE images, 100 (78.1%) of 128 FNH lesions were either slightly hyperintense or isointense to the surrounding parenchyma, while the remaining 28 lesions were either not visible ($n = 27$) or were atypically slightly hypointense ($n = 1$). On the corresponding precontrast T1-weighted GRE images, 99 (77.3%) lesions were isointense or slightly hypointense. Among the visible lesions, all but four showed homogeneous signal intensity. A hyperintense central scar was apparent on precontrast T2-weighted images in 36 FNH lesions, of which 29 were detected in 60 lesions that were 3 cm or larger in size and seven were detected in 68 lesions smaller than 3 cm in size. Hypointense central scars on precontrast T1-weighted GRE images were detected in 40 lesions, with 34 seen in 60 lesions 3 cm and larger in size and six seen in 68 lesions smaller than 3 cm in size. No central scars were seen in any lesion that was smaller than 2 cm in size.

Concerning HA and LA, 99 (92.5%) of 107 lesions were either slightly hyperintense or isointense to the surrounding parenchyma on precontrast T2-weighted images, seven lesions were not visible, and one lesion was slightly hypointense. A more varied behavior was noted on precontrast T1-weighted GRE images, with 79 (73.8%) lesions appearing isointense or slightly hypointense and 21 (19.6%) lesions appearing slightly hyperintense. Compared with FNH, fewer visible HAs demonstrated homogeneous signal intensity on precontrast images. Overall, 10 of 30 visible HAs showed heterogeneous signal intensity suggestive of intralesional hemorrhage, fat, or necrosis, and 20 demonstrated homogeneous signal intensity. Among the 75 LA lesions, all but six showed homogeneous signal intensity on precontrast images.

Based solely on lesion appearance on precontrast images, a tentative diagnosis was possible in 40 (31.3%) of 128 FNHs, 10 of (31.2%) 32 HAs, and six (8.0%) of 75 LA lesions. For the remaining 179 (76.2%) of 235 lesions, results of unenhanced imaging did not provide sufficient information for differential diagnosis.

Postcontrast Dynamic Phase Imaging

During the arterial phase, 122 of 128 FNHs showed marked homogeneous hyperintensity to the surrounding normal liver parenchyma, while the remaining six lesions showed heterogeneous hyperintensity. Slight hyperintensity that persisted into the portal venous and equilibrium phases was noted for 60 (46.9%) and 42 (32.8%) lesions, respectively (Figs 1–4). All but one of the remaining lesions were isointense in the portal venous and equilibrium phases; the one exception was a small (<1-cm) FNH, which had a very slight hypointense appearance. A hypointense central scar was noted in 48 of 128 lesions on arterial phase images, of which 36 were seen in lesions 3 cm and larger (Fig 1c) and 12 were seen in lesions smaller than 3 cm but larger than 2 cm in size. Of the 48 hypointense scars, 45 were seen as hyperintense during the equilibrium phase. The remaining three hypoin-

Morphologic Characteristics and Enhancement Patterns of FNH, HA, and LA

Signal Intensity	Precontrast Phase		Postcontrast Dynamic Phase			Delayed Phase 1–3 Hours
	T2-weighted	T1-weighted	Arterial	Portal Venous	Equilibrium	
			FNH (n = 128)			
Hyperintense	46 (35.9)	0	128 (100)	60 (46.9)	42 (32.8)	87 (68.0)
Isointense	54 (42.2)	61 (47.7)	0	67 (52.3)	85 (66.4)	37 (28.9)
Hypointense	1 (0.8)	38 (29.7)	0	1 (0.8)	1 (0.8)	4 (3.1)
Not visible	27 (21.1)	29 (22.7)	0	0	0	0
			HA (n = 32)			
Hyperintense	21 (65.6)	8 (25.0)	32 (100)	10 (31.3)	7 (21.9)	0
Isointense	7 (21.9)	12 (37.5)	0	11 (34.4)	11 (34.4)	0
Hypointense	1 (3.1)	10 (31.3)	0	11 (34.4)	14 (43.8)	32 (100)
Not visible	3 (9.4)	2 (6.3)	0	0	0	0
			LA (n = 75)			
Hyperintense	43 (57.3)	13 (17.3)	71 (94.7)	42 (56.0)	8 (10.7)	0
Isointense	28 (37.3)	46 (61.3)	4 (5.3)	24 (32.0)	56 (74.7)	0
Hypointense	0	11 (14.7)	0	9 (12.0)	11 (14.7)	75 (100)
Not visible	4 (5.3)	5 (6.7)	0	0	0	0
			HA and LA (n = 107)			
Hyperintense	64 (59.8)	21 (19.6)	103 (96.3)	52 (48.6)	15 (14.0)	0
Isointense	35 (32.7)	58 (54.2)	4 (3.7)	35 (32.7)	67 (62.6)	0
Hypointense	1 (0.9)	21 (19.6)	0	20 (18.7)	25 (23.4)	107 (100)
Not visible	7 (6.5)	7 (6.5)	0	0	0	0

Note.—Data are the number of lesions. Data in parentheses are percentages.

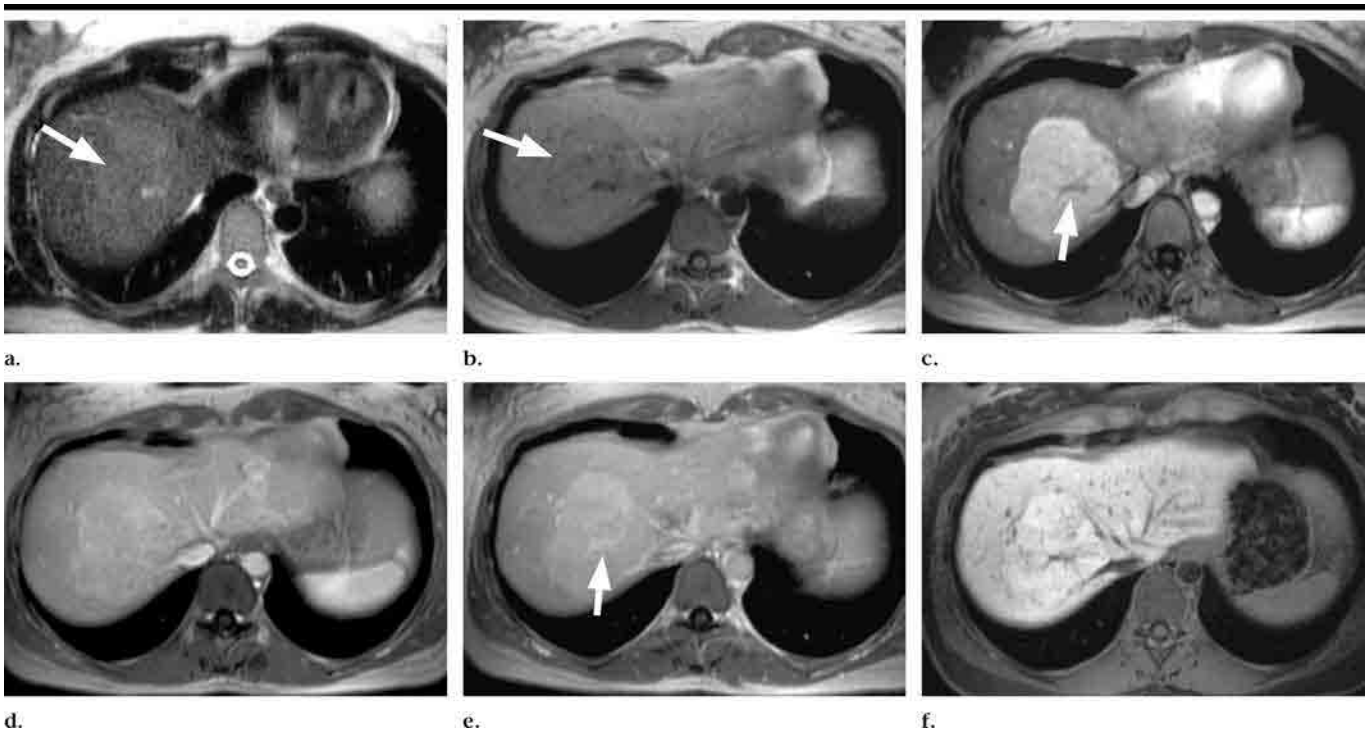

Figure 1. MR images in a 38-year-old woman with typical FNH, pain in upper abdomen, and 10-year history of oral contraceptive use. **(a)** Transverse T2-weighted half-Fourier RARE (∞/74, 180° flip angle) image shows a faintly hyperintense lesion (arrow) of approximately 8 cm in liver segment VIII. **(b)** On unenhanced transverse T1-weighted GRE (140/4.7, 70° flip angle) image, the lesion (arrow) is very faintly hypointense to the surrounding parenchyma. **(c)** On corresponding postcontrast arterial phase T1-weighted GRE image, the lesion demonstrates strong homogeneous enhancement and retains a faint hyperintensity during subsequent **(d)** portal venous and **(e)** equilibrium phases. A characteristic central scar (arrow in **c** and **e**) is clearly seen as hypointense in arterial phase and as hyperintense in equilibrium phase. **(f)** Although FNH diagnosis is likely based on dynamic phase images alone, confirmation comes from a marked hyperintense appearance of the lesion on hepatobiliary phase fat-suppressed T1-weighted GRE image acquired 3 hours after gadobenate dimeglumine injection. The central scar is again hypointense during delayed hepatobiliary phase.

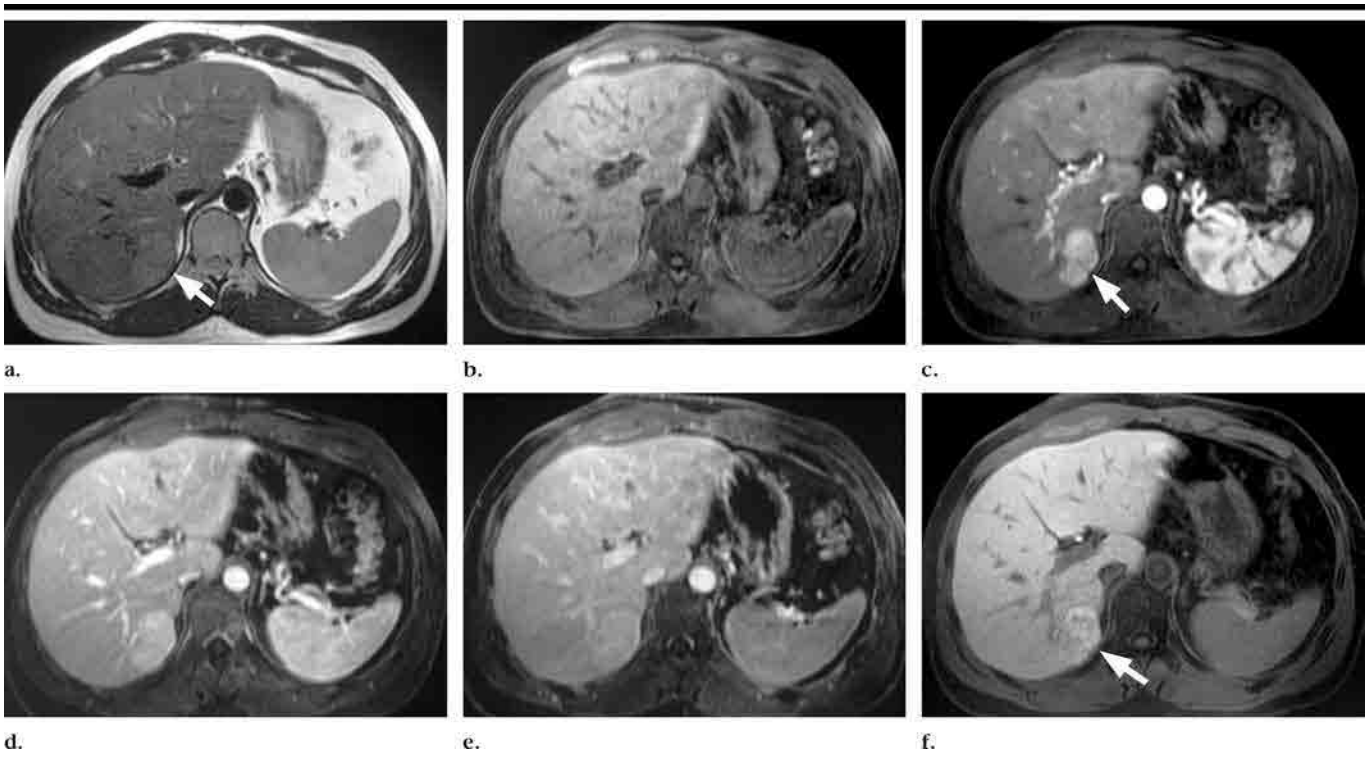

Figure 2. MR images in a 30-year-old asymptomatic man with FNH. **(a)** Transverse T2-weighted fast spin-echo (4000/90, 150° flip angle) image reveals a faintly hyperintense lesion (arrow) of approximately 5 cm in liver segment VII. **(b)** On unenhanced transverse T1-weighted fat-suppressed VIBE (6.2/2.5, 15° flip angle) image, the lesion is very faintly hypointense. **(c)** On corresponding postcontrast arterial phase T1-weighted VIBE image, the lesion (arrow) demonstrates strong enhancement that persists into **(d)** portal venous phase. **(e)** On corresponding equilibrium phase T1-weighted VIBE image, the lesion is iso- to slightly hyperintense to the surrounding normal liver parenchyma. No central scar is apparent, and accurate differentiation from HA is not possible on the basis of unenhanced and postcontrast dynamic series of images. **(f)** On transverse T1-weighted fat-suppressed GRE (140/4.7, 70° flip angle) image acquired 3 hours after injection of gadobenate dimeglumine, the lesion (arrow) is homogeneously hyperintense to the normal parenchyma. Although a clear central scar is not evident, the hyperintense appearance of the lesion is sufficient for the diagnosis of a benign lesion for which conservative management is indicated.

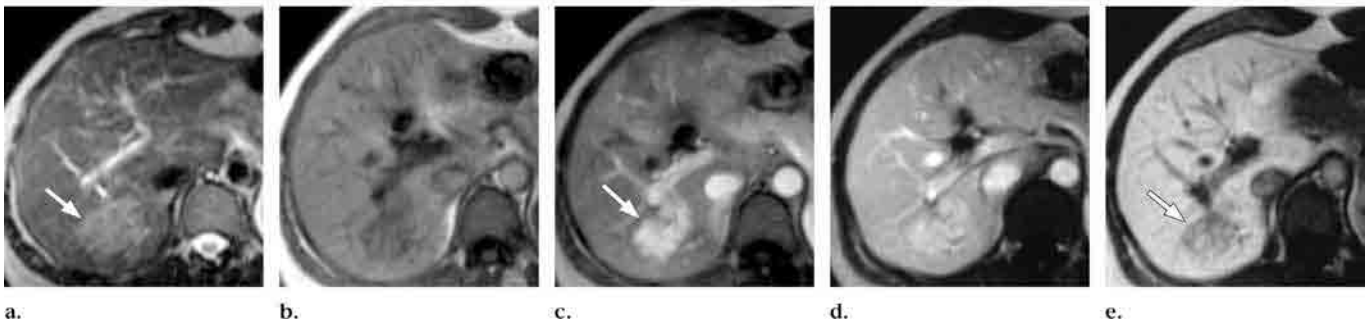

Figure 3. MR images in a 53-year-old asymptomatic woman with atypical FNH. **(a)** Transverse T2-weighted fast spin-echo (4000/108, 150° flip angle) image reveals a faintly hyperintense lesion (arrow) of approximately 7 cm in liver segment VI. **(b)** On unenhanced transverse T1-weighted GRE (160/4.7, 70° flip angle) image, the lesion is clearly hypointense to the surrounding parenchyma. **(c)** On corresponding postcontrast arterial phase T1-weighted GRE image, the lesion (arrow) demonstrates strong homogeneous enhancement and appears isointense and faintly hyperintense during subsequent **(d)** portal venous phase. No central scar is apparent, and accurate diagnosis is difficult on the basis of unenhanced and dynamic phase images alone. **(e)** On corresponding T1-weighted GRE image acquired 3 hours after injection of gadobenate dimeglumine, the lesion (arrow) has an atypical appearance with nodular areas of isointensity and slight hyperintensity interspersed with abundant internal hypointense septa, which results in the lesion appearing predominantly hypointense relative to the surrounding normal parenchyma. A characteristic central scar is not apparent and lesion biopsy is indicated.

tense scars were either isointense (n = 1) or retained an atypical hypointense appearance during the equilibrium phase (n = 2, both in lesions <3 cm in size). Four atypical hyperintense scars were also noted in four lesions on arterial phase images. These scars were either hyperintense (n = 3) or isointense (n = 1) on equilibrium phase images. A total of 49 hyperintense scars were detected on equilibrium phase images, of which 38 were in lesions 3 cm or larger and 11 were

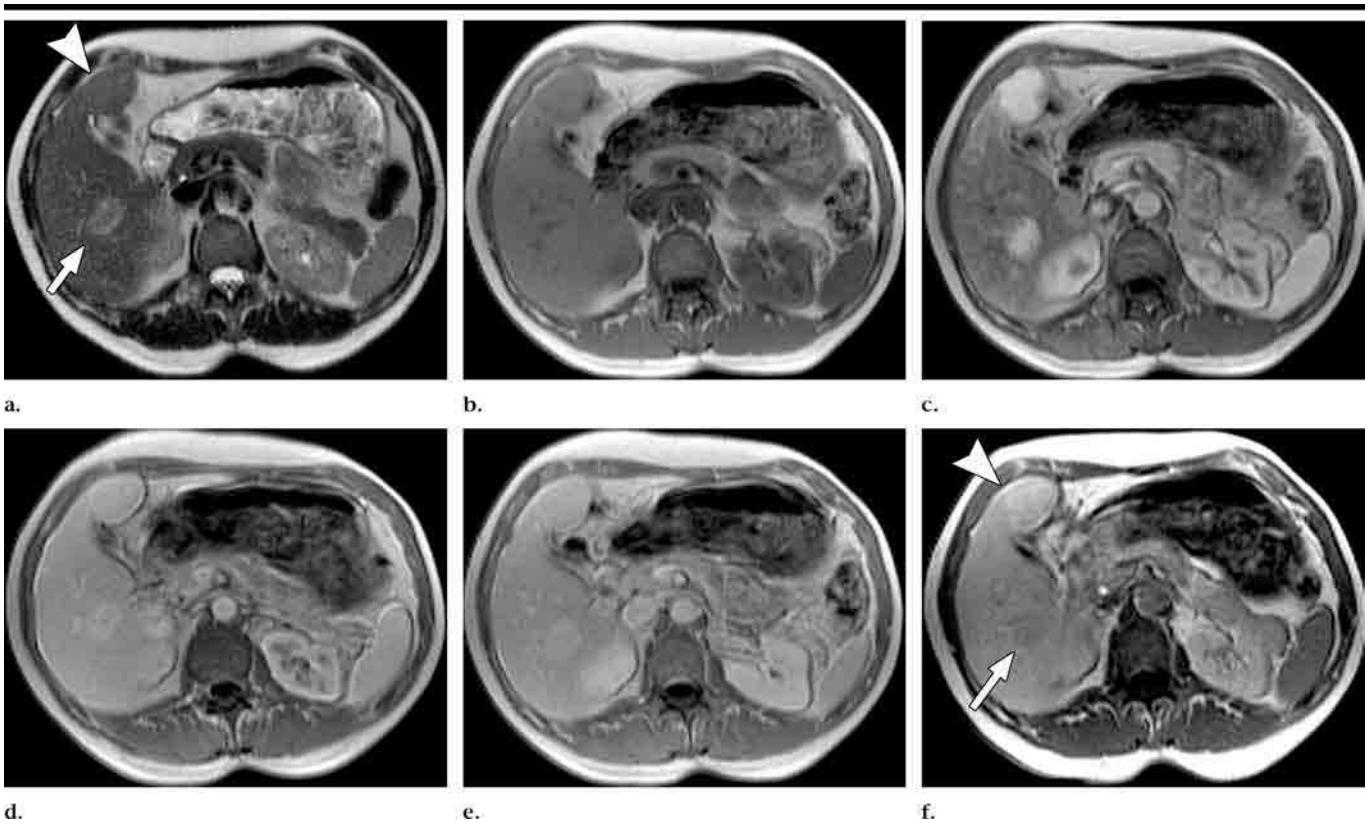

Figure 4. MR images in a 56-year-old asymptomatic woman with both FNH and HA and undergoing hormone replacement therapy. **(a)** Transverse T2-weighted half-Fourier RARE (∞/74, 180° flip angle) image reveals two lesions, one of which (arrow) is slightly hyperintense to the surrounding normal parenchyma in liver segment VI and the other (arrowhead) is isointense in liver segment IV. **(b)** Both lesions are isointense on unenhanced transverse T1-weighted GRE (140/4.7, 70° flip angle) image but demonstrate strong enhancement on **(c)** the corresponding arterial phase T1-weighted GRE image and persistent hyperintensity in **(d)** portal venous and **(e)** equilibrium phases. Postcontrast dynamic series of acquisitions confirm the hypervascular nature of the lesions, but accurate differential diagnosis is not possible. **(f)** On corresponding hepatobiliary phase T1-weighted GRE image acquired 2 hours after injection of gadobenate dimeglumine, the FNH (arrowhead) is hyperintense to the normal parenchyma and the HA (arrow) is hypointense. The hypointense appearance of HA indicates that this lesion should be considered for resection, while the hyperintense appearance of FNH indicates a true benign lesion requiring only follow-up.

in lesions smaller than 3 cm but larger than 2 cm in size. Overall, a diagnostically relevant central scar was noted in 53 of 128 lesions in one or more phases of the dynamic series. The 75 FNH lesions in which no central scar was evident on dynamic phase images comprised 54 of 68 lesions smaller than 3 cm and 21 of 60 lesions 3 cm and larger in size (Figs 2c, 3c). Notably, a central scar was observed in only one of the six FNHs that demonstrated heterogeneous hyperintensity during the dynamic phase.

The enhancement behavior of HA and LA was similar to that of FNH on dynamic phase images (Figs 4–6). Overall, 103 (96.3%) of 107 lesions (including all solitary HAs) were markedly hyperintense to the normal parenchyma on arterial phase images, while the remaining four small (1-cm) LA lesions appeared isointense. A similar pattern of enhancement to that occurring with FNH was observed for HA and LA lesions during the subsequent portal venous and equilibrium phases. By the equilibrium phase, 15 (14.0%) of 107 lesions (comprising seven of 32 HAs and eight of 75 LA lesions) retained a hyperintense appearance (Fig 4e), while 67 (62.6%) lesions were isointense. Compared with FNH, a higher proportion of HA and LA lesions (25 of 107 lesions, comprising 14 of 32 HA and 11 of 75 LA lesions) appeared slightly hypointense during the equilibrium phase. A heterogeneous appearance suggestive of areas of nonenhancing necrosis or hemorrhage was noted for 10 HA and seven LA lesions. The remaining 22 HA and 68 LA lesions demonstrated homogeneous enhancement during the dynamic phase.

Based on the presence of characteristic lesion features during the dynamic phase of contrast enhancement, a tentative diagnosis was possible for 53 (41.4%) of 128 FNH and 17 (15.9%) of 107 HA and LA lesions. Because of overlapping contrast enhancement behavior and the absence of characteristic features in a large number of lesions, confident differential diagnosis was not possible for 165 (70.2%) of 235 lesions on the basis of dynamic phase imaging alone. The number of lesions for which a confident differential diagnosis was possible was not altered with the combined assessment of both unenhanced and dynamic phase images.

Postcontrast Hepatobiliary Phase Imaging

On delayed phase T1-weighted GRE images acquired at 1–3 hours after administration of gadobenate dimeglumine, 124 (96.9%) of 128 FNH lesions appeared either hyperintense (n = 87, 68.0%) or isointense (n = 37, 28.9%) to the surrounding enhanced normal parenchyma (Figs 1f, 2f, 4f). An atypical

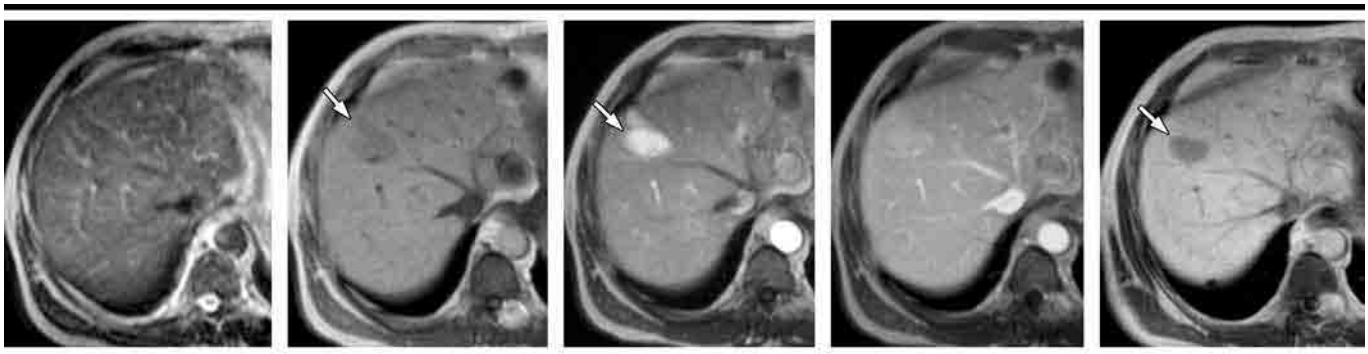

Figure 5. MR images in a 50-year-old asymptomatic man with HA. **(a)** No lesion is evident on unenhanced transverse T2-weighted fast spin-echo (4000/90, 150° flip angle) image. **(b)** On unenhanced transverse T1-weighted GRE (160/4.7, 70° flip angle) image, a faintly hypointense lesion (arrow) of approximately 3 cm is evident in liver segment VIII. **(c)** On corresponding postcontrast arterial phase T1-weighted GRE image, the lesion (arrow) demonstrates strong enhancement but appears only very slightly hyperintense to the surrounding normal liver parenchyma during **(d)** portal venous phase. Accurate differentiation of HA from FNH is not possible on the basis of only unenhanced and postcontrast dynamic phase images. **(e)** On corresponding T1-weighted GRE image acquired 3 hours after injection of gadobenate dimeglumine, the lesion (arrow) is homogeneously hypointense to the normal parenchyma, which enables the differential diagnosis of FNH to be excluded. Although alternative diagnosis such as hypervascular hepatocellular carcinoma or hypervascular metastasis cannot be excluded, the hypointense appearance at hepatobiliary phase imaging is sufficient to indicate a lesion for which resection should be considered.

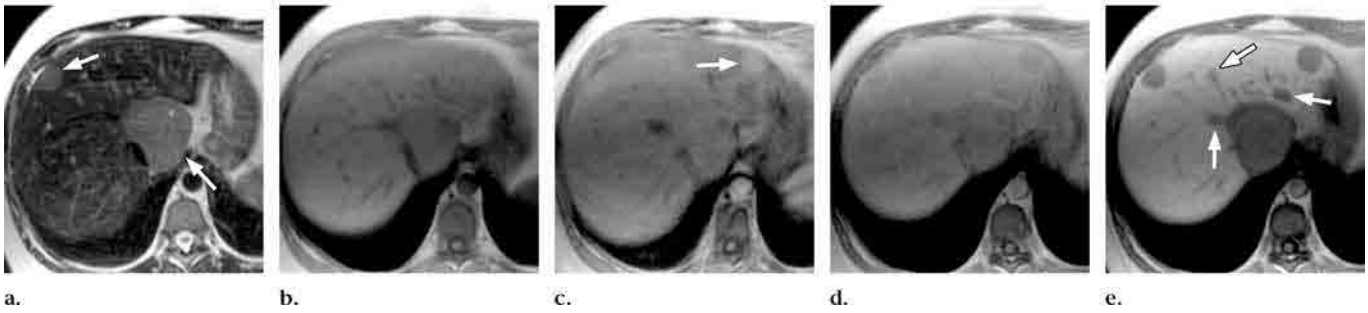

Figure 6. MR images in a 45-year-old woman with LA, a 6-year history of oral contraceptive use, and pain in the upper abdomen. **(a)** Transverse T2-weighted half-Fourier RARE (∞/74, 180° flip angle) image clearly reveals two hyperintense lesions (arrows). **(b)** On unenhanced transverse T1-weighted GRE (156/4.7, 70° flip angle) image, these lesions are isointense to the normal liver parenchyma. **(c)** Only minimal enhancement of these lesions is seen on corresponding T1-weighted postcontrast arterial phase GRE image, although a third hyperintense lesion (arrow) is seen. **(d)** These lesions are already faintly hypointense to the normal liver parenchyma during portal venous phase. **(e)** During hepatobiliary phase at 3 hours after gadobenate dimeglumine administration, these lesions and other very small lesions (arrows) are very clearly hypointense to the surrounding enhanced normal liver parenchyma.

slightly hypointense nodular appearance compared to the surrounding parenchyma was noted for the remaining four (3.1%) FNH lesions (Fig 3e). In all cases in which delayed images were acquired at two or more time points between 1 and 3 hours after injection, lesions that were hyperintense to the normal parenchyma after 1 hour were equally or slightly more hyperintense at later time points up to 3 hours after injection. Similarly, lesions that were isointense after 1 hour were also isointense subsequently. The appearance of FNH lesions was considered to be homogeneous in 87 (68.0%) of 128 lesions, slightly heterogeneous in 23 (18.0%) lesions, and with peripheral enhancement in 18 (14.0%) lesions. A hypointense central scar was noted in 53 of 128 lesions overall on delayed phase images, with most scars noted in lesions 3 cm and larger in size (38 of 60 lesions). Hypointense central scars were noted in just 15 of 68 FNH lesions smaller than 3 cm in size. In 13 cases, these lesions were 2 cm or larger, and in two cases they were 1.5 cm in size.

Each of the four FNH lesions that were atypically slightly hypointense on delayed images after administration of gadobenate dimeglumine had a nodular appearance that consisted of internal areas that enhanced at least to the same extent as the surrounding normal parenchyma interspersed by abundant internal hypointense fibrous septa (Fig 3e). The presence of hypointense fibrous septa resulted in these lesions having a predominantly hypointense appearance.

Unlike FNH, all 107 (100%) HA and LA lesions were hypointense to the enhanced normal liver parenchyma on postcontrast delayed images. Among HAs, homogeneous hypointensity was noted for 25 of 32 lesions (Figs 4f, 5e) and heterogeneous hypointensity was noted for seven of 32 lesions. All but two of the 75 LA lesions were homogeneously hypointense (Fig 6e).

The interpretation of lesions was similar on images acquired with and without fat suppression. However, an overall benefit of evaluating delayed phase images with fat suppression was a more pronounced hyperintense appearance of the FNH lesions. Thus, fat-suppressed images generally highlighted the differential enhancement behavior between FNH and HA and LA.

Accuracy

By taking lesion hyperintensity or isointensity on delayed images after gadobenate dimeglumine administration as indicative of FNH (a true-positive lesion) and lesion hypointensity as indicative of HA or LA (a true-negative lesion), the sensitivity, specificity, positive predictive value, negative predictive value, and overall accuracy for the differentiation of FNH from HA and LA were 96.9%, 100%, 100%, 96.4%, and 98.3%, respectively. The difference in appearance between FNH and HA and LA lesions on postcontrast delayed images was highly significant ($\chi^2 = 219.5$, $df = 2$, $P < .001$). Additional analyses performed to take into account possible correlations between multiple lesions in individual patients produced similar findings: Highly significant differences between FNH and HA and LA lesions were noted with both χ^2 analysis of just a single lesion in each patient ($\chi^2 = 95.4$, $df = 1$, $P < .001$) and with an overall analysis by using generalized estimating equation methods ($Z = 6.81$, $P \leq .0001$). On the basis of these results and the sample size, the computed power of the test exceeded 99.9%.

DISCUSSION

Although FNH, HA, and LA liver lesions are all benign, HA and LA lesions are frequent candidates for surgical intervention because of their potential for malignant transformation and, in the case of larger (>5-cm) lesions in particular, their propensity for spontaneous rupture and hemorrhage (3,4,7–17). The clinical need is therefore to differentiate these lesions accurately at noninvasive diagnostic imaging without recourse to lesion biopsy. Unfortunately, the imaging techniques available at present in routine practice are not always specific for the differential diagnosis of these lesions (3,8,9,17,23). Furthermore, the comparatively frequent occurrence of atypical lesions, which do not possess morphologic features considered characteristic for these lesions, may further complicate the diagnosis.

A recent study performed to define the use of gadobenate dimeglumine for the characterization of FNH revealed that 21% of the lesions evaluated were morphologically atypical (36). Authors of earlier studies suggested that 50% or more of FNH and HA lesions may not possess the features considered characteristic for these lesions (11,16,20,22). The difficulty in differentiating FNH from noncomplicated HA on the basis of unenhanced T1- and T2-weighted images or enhanced T1-weighted images after use of a conventional gadolinium-based contrast agent is well known. Both types of lesions enhance strongly during the arterial phase and then either retain a hyperintense appearance or demonstrate isointensity with the normal liver parenchyma during subsequent portal venous and equilibrium phases. Findings of the present study reveal that while FNH and HA and LA lesions cannot be differentiated reliably on unenhanced and postcontrast dynamic phase MR images, highly accurate differentiation of these lesions is possible on delayed images acquired at 1–3 hours after the administration of gadobenate dimeglumine. Specifically, the overall accuracy for the differentiation of FNH from HA and LA on the basis of delayed hepatobiliary phase images alone was 98.3%. Of the 235 lesions evaluated, just four (3.1%) of 128 relatively small FNHs demonstrated atypical hypointensity on hepatobiliary phase images. In each case, the lesion was nodular in appearance with internal areas of characteristic iso- or hyperintensity interspersed by abundant hypointense internal fibrous septa. Histologic findings confirmed the FNH character of these lesions without revealing any obvious differences from histologically confirmed FNH that demonstrate typical homogeneous hyperintensity on delayed images.

The overall different enhancement behavior of FNH and of HA and LA on postcontrast delayed images can be ascribed to the different structural and functional features of the lesions and to the capacity for uptake of the Gd-BOPTA contrast-effective chelate of gadobenate dimeglumine by lesions with functioning hepatocytes. The Gd-BOPTA chelate of gadobenate dimeglumine, unlike the Gd chelates of other available gadolinium-based agents, has a dual route of elimination through both the renal and hepatobiliary pathways (29,30,33). Approximately 3%–5% of the injected dose is taken up into functioning hepatocytes and is eliminated into the bile across the sinusoidal membrane by means of the adenosine triphosphate–dependent canalicular multispecific organic anion transporter peptide that transports bilirubin (31,32). Thus, lesions containing functioning hepatocytes in which hepatobiliary metabolism is largely unaltered compared with that of normal hepatocytes may be expected to take up the Gd-BOPTA chelate in a similar manner and to excrete it into the bile. Such lesions are typically benign (eg, FNH and nodular regenerative hyperplasia) and usually appear at least isointense to the normal liver parenchyma on postcontrast delayed MR images (36,40). Conversely, lesions that do not contain functioning hepatocytes in which hepatobiliary metabolism is blocked or inhibited are generally unable to take up and excrete Gd-BOPTA into the bile. Such lesions are typically malignant (eg, hepatocellular carcinoma, metastases) and usually appear hypointense to the normal liver parenchyma on postcontrast delayed MR images. Previous study findings have confirmed that malignant lesions generally appear hypointense on delayed phase images (33,35,41,42); only a few well-differentiated hepatocellular carcinomas have been shown to retain sufficient hepatocytic functionality to take up Gd-BOPTA (42).

Both FNH and HA or LA lesions are hypervascular, which accounts for their similar behavior on postcontrast dynamic phase images when lesion enhancement is entirely due to differential contrast agent distribution between the lesion and normal liver parenchyma in the initial 2–3 minutes after contrast agent injection. In the case of FNH, this lesion is considered to be the result of a hyperplastic response to the presence of a preexisting vascular malformation and occurs when increased arterial flow hyperperfuses the local parenchyma, leading to secondary hepatocellular hyperplasia (1). Histologically, FNH is characterized by the presence of normal hepatocytes with a malformed biliary system in which the primary bile ductules are blind-ending and have no connection to the larger bile ducts. As a consequence, biliary excretion is slowed compared with that occurring in normal hepatocytes (2). HA and LA, on the other hand, are composed of cordlike arrangements of cells structured in large plates separated by dilated sinusoids (43). These sinusoids are the equivalent of thin-walled capillaries. HA and LA differ from FNH in lacking a portal venous supply; these lesions are perfused solely by arterial pressure deriving from peripheral arterial feeding vessels (40). The hypervascular nature of HA and LA is due principally to the extensive sinusoids and feeding arteries and to the poor connective tissue support, which is a primary factor in predisposing the lesion to hemorrhage.

The key histologic feature that enables HA and LA to be distinguished from FNH on postcontrast delayed phase images is that, whereas FNH possess malformed

biliary ductules, HA and LA do not possess biliary ductules at all (2,18). Hence, bilirubin metabolism is blocked within HA and LA, as confirmed by the absence of bile within resected lesions (11). In the case of FNH, it is likely that the iso- or hyperintense appearance of lesions on delayed images reflects a normal ability to take up Gd-BOPTA and a normal ability to transport it across the sinusoidal membrane into the primary bile ductules. However, the absence of any connection between the malformed blind-ending primary ductules and the larger bile ducts thereafter impairs normal hepatobiliary elimination and results in an accumulation of Gd-BOPTA within the ductules and hence persistent enhancement of the lesion. Over time, as hepatobiliary elimination from the surrounding normal hepatocytes leads to continually decreasing signal intensity enhancement in normal parenchyma, the hyperintense appearance of FNH would be expected to increase, augmented by the re-uptake of Gd-BOPTA from the blind-ending biliary ductules into the hepatocytes of the lesion. Observations in this study and in a previous study (36) have confirmed that the hyperintensity of FNH relative to the normal liver parenchyma is frequently increased on images acquired 3 hours after gadobenate dimeglumine administration compared with that on images acquired 1 hour after administration.

In the case of HA and LA, it is reasonable to assume that the absence of biliary ductules within the lesion results in altered hepatocellular transport compared with that occurring in normal hepatocytes. Thus, while the mechanism of Gd-BOPTA entry into the hepatocytes of HA and LA may be unaltered, the absence of an intracellular transport gradient due to lack of any active transport across the sinusoidal membrane would manifest as hypointensity against normal enhanced parenchyma on delayed images, in which enhancement is derived from the presence of Gd-BOPTA in both the hepatocytes and the adjacent biliary system. Unfortunately, despite numerous studies aimed at elucidating the mechanism of hepatocellular transport (31,32), it is as yet unclear whether Gd-BOPTA entry into hepatocytes occurs passively or by means of an organic anion transporting peptide (32). Further work is required to determine whether the hypointense appearance of HA and LA on delayed images reflects solely the lack of intracellular transport in combination with free entry into and out of hepatocytes or whether entry of Gd-BOPTA across the hepatocellular membrane is blocked completely.

As with hypointense malignant lesions, the hypointense appearance of HA and LA on postcontrast delayed images can be taken as indicating a possible candidate for surgical resection. However, it is also important to be able to distinguish these lesions from other focal lesions that typically appear hypointense in the delayed phase after gadobenate dimeglumine administration such as capillary hemangioma, hypervascular metastases, and epithelioid hemangioendothelioma. In the case of capillary hemangioma, accurate differentiation is usually possible because of the strongly hyperintense appearance of these lesions on T2-weighted images, their much stronger enhancement on T1-weighted arterial phase GRE images, and the fact that capillary hemangiomas are usually smaller than 2 cm in size (44).

Hypervascular metastases from primary pancreatic islet cell or renal cell cancer or more pertinently in the age group of women likely to have HA, breast cancer, or thyroid cancer may also appear hyperintense in the arterial phase particularly when small in size (45). However, these lesions characteristically appear hyperintense on T2-weighted images, often with central necrotic areas and irregular margins. Moreover, these lesions are often multiple and distinguishable by the absence of fat and hemorrhage, both of which are common in HA (16,18,21). Epithelioid hemangioendothelioma likewise can be distinguished from HA by the absence of fat and calcifications and by the fact that these lesions typically occur in young patients; are usually coalescent in a subcapsular location; and are associated with capsular retraction, abundant central fibrous tissue, and a hypervascular periphery (37,46). On occasion, hypervascular hepatocellular carcinoma in a noncirrhotic liver may also display imaging features that are difficult to differentiate from those of HA. Generally, however, hypervascular hepatocellular carcinomas tend to be more hyperintense than HAs on T2-weighted images and to demonstrate less homogeneous enhancement on postcontrast arterial phase T1-weighted GRE images, depending on size and degree of differentiation (47). Furthermore, hypervascular hepatocellular carcinoma can frequently be distinguished from HA by the presence of a peripheral capsule, which is usually absent in HA.

For the successful differential diagnosis of HA and LA from other hypervascular focal lesions, the possibility to acquire conventional dynamic phase images in addition to delayed hepatobiliary phase images is fundamental. In this regard, the dual imaging capability of gadobenate dimeglumine represents a clear advantage over pure hepatobiliary agents such as the manganese-based agent mangafodipir trisodium, for which only delayed phase imaging is possible (48). Although few studies have been performed with other liver-specific contrast agents, sufficient findings have been reported to suggest that accurate differentiation of FNH from HA may be more problematic. Specifically, both FNH and HA have been reported to enhance on delayed images after the injection of mangafodipir trisodium (49,50), while overlapping uptake of superparamagnetic iron oxide particles precluded confident differential diagnosis of HA from FNH following ferumoxides administration (51,52). In our experience with three patients with four HAs and three patients with LA who each underwent MR imaging on separate occasions with gadobenate dimeglumine, mangafodipir trisodium, and superparamagnetic iron oxide, all adenomas demonstrated uptake of mangafodipir trisodium and appeared isointense to the normal liver parenchyma and thus indistinguishable from FNH. In contrast, after superparamagnetic iron oxide administration, these lesions were either isointense or hyperintense depending on the presence of Kuppfer cells.

Although the results clearly demonstrate that FNH and HA and LA lesions can be distinguished readily on delayed phase images after gadobenate dimeglumine administration, the study is possibly limited in that histologic results were not available for all of the FNH lesions. However, it should be borne in mind that histologic data are typically not acquired in routine practice for focal lesions with morphologic features (ie, central scar) characteristic of FNH. Moreover, in countries in which gadobenate dimeglumine is available, this primary differential criterion is augmented by the characteristic hyper- or isointense appearance on delayed images, which has been shown to permit accurate identification of even atypical FNH lesions (ie, lesions lacking a central scar) (36). In the present study, histologic data were not acquired when the lesion enhancement patterns on dynamic and delayed images were fully consistent with a diagnosis of FNH.

In summary, the present study findings show that highly accurate differen-

tial diagnosis of FNH from HA and LA is achievable on delayed hepatobiliary phase MR images after gadobenate dimeglumine administration. HA and LA lesions are seen as markedly hypointense against the enhanced normal liver parenchyma, which should be taken as indicating a candidate lesion for surgical resection. Conversely, FNH invariably has an iso- or marked hyperintense appearance, which indicates that the lesion is truly benign and that a conservative approach to patient management may suffice. The enhancement pattern on dynamic phase images provides information about the hypervascular nature of both types of lesion and, in the case of HA and LA, can aid in differentiation of these lesions from true hypovascular malignant lesions. Further work is warranted to validate the clinical use of these findings in a more diverse lesion population.

Acknowledgments: The authors thank Ningyan Shen, MD, PhD, and Riccardo Spezia, MSc, for their contributions to the statistical analysis of the data.

References

1. Wanless IR, Mawdsley C, Adams R. On the pathogenesis of focal nodular hyperplasia of the liver. Hepatology 1985; 5:1194–1200.
2. Boulahdour H, Cherqui D, Charlotte F, et al. The hot spot hepatobiliary scan in focal nodular hyperplasia. J Nucl Med 1993; 34: 2105–2110.
3. Cherqui D, Rahmouni A, Charlotte F, et al. Management of focal nodular hyperplasia and hepatocellular adenoma in young women: a series of 41 patients with clinical, radiological, and pathological correlations. Hepatology 1995; 22:1674–1681.
4. Reddy KR, Kligerman S, Levi J, et al. Benign and solid tumors of the liver: relationship to sex, age, size of tumors, and outcome. Am Surg 2001; 67:173–178.
5. Becker YT, Raiford DS, Webb L, Wright JK, Chapman WC, Pinson CW. Rupture and hemorrhage of hepatic focal nodular hyperplasia. Am Surg 1995; 61:210–214.
6. Nagorney DM. Benign hepatic tumors: focal nodular hyperplasia and hepatocellular adenoma. World J Surg 1995; 19:13–18.
7. De Carlis L, Pirotta V, Rondinara GF, et al. Hepatic adenoma and focal nodular hyperplasia: diagnosis and criteria for treatment. Liver Transpl Surg 1997; 3:160–165.
8. Weimann A, Ringe B, Klempnauer J, et al. Benign liver tumors: differential diagnosis and indications for surgery. World J Surg 1997; 21:983–990.
9. Herman P, Pugliese V, Machado MA, et al. Hepatic adenoma and focal nodular hyperplasia: differential diagnosis and treatment. World J Surg 2000; 24:372–376.
10. Charny CK, Jarnagin WR, Schwartz LH, et al. Management of 155 patients with benign liver tumours. Br J Surg 2001; 88: 808–813.
11. Leese T, Farges O, Bismuth H. Liver cell adenomas: 12 years' surgical experience from a specialist hepato-biliary unit. Ann Surg 1988; 208:558–564.
12. Gyorffy EJ, Bredfeldt JE, Black WC. Transformation of hepatic cell adenoma to hepatocellular carcinoma due to oral contraceptive use. Ann Intern Med 1989; 110: 489–490.
13. Tao LC. Oral contraceptive-associated liver cell adenoma and hepatocellular carcinoma: cytomorphology and mechanism of malignant transformation. Cancer 1991; 68:341–347.
14. Foster JH, Berman MM. The malignant transformation of liver cell adenomas. Arch Surg 1994; 129:712–717.
15. Libbrecht L, De Vos R, Cassiman D, Desmet V, Aerts R, Roskams T. Hepatic progenitor cells in hepatocellular adenomas. Am J Surg Pathol 2001; 25:1388–1396.
16. Ichikawa T, Federle MP, Grazioli L, Nalesnik M. Hepatocellular adenoma: multiphasic CT and histopathologic findings in 25 patients. Radiology 2000; 214:861–868.
17. Terkivatan T, de Wilt JH, de Man RA, et al. Indications and long-term outcome of treatment for benign hepatic tumors: a critical appraisal. Arch Surg 2001; 136: 1033–1038.
18. Shortell CK, Schwartz SI. Hepatic adenoma and focal nodular hyperplasia. Surg Gynecol Obstet 1991; 173:426–431.
19. Chen MF. Hepatic resection for benign tumours of the liver. J Gastroenterol Hepatol 2000; 15:587–592.
20. Bioulac-Sage P, Balabaud C, Wanless IR. Diagnosis of focal nodular hyperplasia: not so easy. Am J Surg Pathol 2001; 25: 1322–1325.
21. Chung KY, Mayo-Smith WW, Saini S, Rahmouni A, Golli M, Mathieu D. Hepatocellular adenoma: MR imaging features with pathologic correlation. AJR Am J Roentgenol 1995; 165:303–308.
22. Nguyen BN, Flejou JF, Terris B, Belghiti J, Degott C. Focal nodular hyperplasia of the liver: a comprehensive pathologic study of 305 lesions and recognition of new histologic forms. Am J Surg Pathol 1999; 23: 1441–1454.
23. Bartolozzi C, Lencioni R, Paolicchi A, Moretti M, Armillotta N, Pinto F. Differentiation of hepatocellular adenoma and focal nodular hyperplasia of the liver: comparison of power Doppler imaging and conventional color Doppler sonography. Eur Radiol 1997; 7:1410–1415.
24. Hytiroglou P, Theise ND. Differential diagnosis of hepatocellular nodular lesions. Semin Diagn Pathol 1998; 15:285–299.
25. Semelka RC, Martin DR, Balci C, Lance T. Focal liver lesions: comparison of dual-phase CT and multisequence multiplanar MR imaging including dynamic gadolinium enhancement. J Magn Reson Imaging 2001; 13:397–401.
26. Horton KM, Bluemke DA, Hruban RH, Soyer P, Fishman EK. CT and MR imaging of benign hepatic and biliary tumors. RadioGraphics 1999; 19:431–451.
27. Cavagna FM, Maggioni F, Castelli PM, et al. Gadolinium chelates with weak binding to serum proteins. Invest Radiol 1997; 32:780–796.
28. de Haën C, Cabrini M, Akhnana L, Ratti D, Calabi L, Gozzini L. Gadobenate dimeglumine 0.5M solution for injection (MultiHance): pharmaceutical formulation and physicochemical properties of a new magnetic resonance imaging contrast medium. J Comput Assist Tomogr 1999; 23(suppl 1):S161–S168.
29. Kirchin M, Pirovano G, Spinazzi A. Gadobenate dimeglumine (Gd-BOPTA): an overview. Invest Radiol 1998; 33:798–809.
30. Spinazzi A, Lorusso V, Pirovano G, Kirchin MA. Safety, tolerance, biodistribution and MR imaging enhancement of the liver with gadobenate dimeglumine. Acad Radiol 1999; 6:282–291.
31. Pascolo L, Petrovic S, Cupelli F, et al. Abc protein transport of MRI contrast agents in canalicular rat liver plasma vesicles and yeast vacuoles. Biochem Biophys Res Commun 2001; 282:60–66.
32. Pastor CM, Planchamp C, Pochon S, et al. Kinetics of gadobenate dimeglumine in isolated perfused rat liver: MR imaging evaluation. Radiology 2003; 229:119–125.
33. Spinazzi A, Lorusso V, Pirovano G, Taroni P, Kirchin M, Davies A. MultiHance clinical pharmacology: biodistribution and MR enhancement of the liver. Acad Radiol 1998; 5(suppl 1):S86–S89.
34. Petersein J, Spinazzi A, Giovagnoni A, et al. Evaluation of the efficacy of gadobenate dimeglumine in MR imaging of focal liver lesions: a multicenter phase III clinical study. Radiology 2000; 215:727–736.
35. Pirovano G, Vanzulli A, Marti-Bonmati L, et al. Evaluation of the accuracy of gadobenate dimeglumine-enhanced MR imaging in the detection and characterization of focal liver lesions. AJR Am J Roentgenol 2000; 175:1111–1120.
36. Grazioli L, Morana G, Federle MP, et al. Focal nodular hyperplasia: morphological and functional information from MR imaging with gadobenate dimeglumine. Radiology 2001; 221:731–739.
37. Grazioli L, Federle MP, Ichikawa T, Balzano E, Nalesnik M, Madariaga J. Liver adenomatosis: clinical, histopathologic, and imaging findings in 15 patients. Radiology 2000; 216:395–402.
38. Chiche L, Dao T, Salame E, et al. Liver adenomatosis: reappraisal, diagnosis, and surgical management—eight new cases and review of the literature. Ann Surg 2000; 231:74–81.
39. Grazioli L, Federle MP, Brancatelli G, Ichikawa T, Olivetti L, Blachar A. Hepatic adenomas: imaging and pathologic findings. RadioGraphics 2001; 21:877–892.
40. Schneider G, Grazioli L, Saini S, eds. Imaging of benign focal liver lesions. In: MRI of the liver: imaging techniques, contrast enhancement, differential diagnosis. Milan, Italy: Springer-Verlag, 2003; 105–170.
41. Caudana R, Morana G, Pirovano G, et al. Focal malignant hepatic lesions: MR imaging enhanced with gadolinium benzyloxypropionictetra-acetate (BOPTA)—preliminary results of phase II clinical application. Radiology 1996; 199:513–520.
42. Grazioli L, Morana G, Caudana R et al. Hepatocellular carcinoma: correlation between gadobenate dimeglumine-enhanced MRI and pathologic findings. Invest Radiol 2000; 35:25–34.
43. Molina EG, Schiff ER. Benign solid lesion of the liver. In: Schiff's diseases of the liver. 8th ed. Vol II. Philadelphia, Pa: Lippincott-Raven, 1999; 1254–1257.
44. Semelka RC, Brown ED, Ascher SM, et al. Hepatic hemangiomas: a multi-institu-

tional study of appearance on T2-weighted and serial gadolinium-enhanced gradient-echo MR images. Radiology 1994; 192: 401–406.
45. Danet IM, Semelka RC, Leonardou P, et al. Spectrum of MRI appearances of untreated metastases of the liver. AJR Am J Roentgenol 2003; 181:809–817.
46. Miller WJ, Dodd GD 3rd, Federle MP, Baron RL. Epithelioid hemangioendothelioma of the liver: imaging findings with pathologic correlation. AJR Am J Roentgenol 1992; 159:53–57.
47. Kadoya M, Matsui O, Takashima T, Nonomura A. Hepatocellular carcinoma: correlation of MR imaging and histopathologic findings. Radiology 1992; 183:819–825.
48. Kettritz U, Schlund JF, Wilbur K, Eisenberg LB, Semelka RC. Comparison of gadolinium chelates with manganese-DPDP for liver lesion detection and characterization: preliminary results. Magn Reson Imaging 1996; 14:1185–1190.
49. Coffin CM, Diche T, Mahfouz A, et al. Benign and malignant hepatocellular tumors: evaluation of tumoral enhancement after mangafodipir trisodium injection on MR imaging. Eur Radiol 1999; 9:444–449.
50. King LJ, Burkill GJ, Scurr ED, Vlavianos P, Murray-Lyons I, Healy JC. MnDPDP enhanced magnetic resonance imaging of focal liver lesions. Clin Radiol 2002; 57:1047–1057.
51. Vogl TJ, Hammerstingl R, Schwarz W, et al. Superparamagnetic iron oxide–enhanced versus gadolinium-enhanced MR imaging for differential diagnosis of focal liver lesions. Radiology 1996; 198:881–887.
52. Beets-Tan RG, Van Engelshoven JM, Greve JW. Hepatic adenoma and focal nodular hyperplasia: MR findings with superparamagnetic iron oxide-enhanced MRI. Clin Imaging 1998; 22:211–215.